Multivariate Adaptive Sampling of Parameterized Antenna Responses

Ngoy Mutonkole, and Dirk I. L. de Villiers, *Senior Member, IEEE*

***Abstract*—We present a robust method to adaptively construct parameterized models of the full radiation patterns of antennas and the associated S-parameters. The method sequentially selects points (geometric parameters of the antenna and frequency) such that an accurate model is obtained over a constrained multivariate parameter space. The algorithm consists of a balance between exploration and exploitation of the parameter space, resulting in a near optimal coverage of the design space, with some emphasis being placed in regions of the parameter space where the patterns or S-parameters vary rapidly. In addition, the technique is equipped with a measure of absolute error control. The proposed method is validated through pertinent numerical examples.**

***Index Terms*—Adaptive sampling, antenna radiation patterns, modeling.**

I. Introduction

MODERN antenna design is often optimization based, and thus requires repeated electromagnetic (EM) simulations of the antenna for different combinations of geometric parameters. Optimization is a computationally expensive task due to the typically large computational cost associated with EM simulations.

To address this challenge, several computationally cheap surrogate models of the antenna's response have been studied. In [1], an efficient Kriging model that is enhanced with gradient information, is used to model antenna responses. A Bayesian approach is used in [2] for multivariate S-parameter modeling. Variable fidelity techniques, using co-Kriging as the modeling method, have been discussed in [3], [4]. Another variant of variable fidelity methods is investigated in [5]. The techniques in [1]–[5], among others, aim to reduce the computational cost of antenna design by reducing the number of accurate EM simulations required during the optimization of the antenna under consideration. All the above methods develop models for a single figure of merit and models have to be extracted at each frequency of interest, thus implying repeated EM simulations for a given combination of geometric design variables. Moreover, in the case of a multi-objective design, different models have to be constructed for different figures of merit (e.g., gain, cross-polarization).

Manuscript received xxx xx, 201x; revised xxx xx, 201x; accepted xxx xx, 201x. Date of publication xxx xx, 201x; date of current version xxx xx, 201x.

This work was financially supported by the South African Research Chair Initiative of the Department of Science and Technology and the NRF. Opinions expressed and conclusions arrived at are those of the authors.

Ngoy Mutonkole and Dirk I. L. de Villiers are with the Department of Electrical and Electronic Engineering, Stellenbosch University, Stellenbosch 7600, South Africa (e-mail: ngoymutonx@gmail.com, ddv@sun.ac.za).

Digital object identifier xxx

Recently, a parametric modeling technique that yields accurate full radiation patterns, as a function of the antenna's geometric variables, has been proposed [6]. This method makes use of the characteristic basis function pattern (CBFP) method [7]–[9], where the expansion coefficients are parameterized with respect to the antenna's geometric variables. The techniques in [1]–[6] make use of a pre-allocated grid, typically through a latin hypercube sampling (LHS) algorithm [10], of EM data from which models are extracted. Such a pre-allocation scheme may result in over/under-sampling of the design space, resulting in either inaccurate models or in an unnecessarily lengthy model building process. The pre-allocation of points may also require some knowledge of the dynamic behavior of the considered antenna. There is thus a need for a method that can be executed blindly and adaptively in order to efficiently build accurate radiation pattern models.

An adaptive frequency sampling method to model radiation pattern variations as a function of frequency is reported in [11], where a robust and accurate technique was demonstrated on different antennas over a wide frequency bandwidth while requiring EM simulations at only a few frequency points. The method in [11] involved only a single variable (frequency).

This paper presents a multivariate adaptive sampling algorithm to model the radiation pattern and the associated S-parameters of antennas as a function of geometric variables and frequency. The presented method is an extension of [11] to the general multivariate case, and is guaranteed to converge to an accurate model, with a fully controllable error, within a modest number of iterations. The proposed technique addresses the over/under-sampling issues elucidated earlier and can be executed without *a priori* knowledge of the antenna's behavior over a given design space. This paper represents an improvement on the approaches in [6], [11] and is, to our knowledge, the first adaptive sampling method for parameterized full radiation patterns. The proposed algorithm is easily extended to include S-parameter variations, thereby providing a full characterization of an antenna using a minimum number of EM simulations. Pertinent numerical examples are provided to validate the proposed method.

This paper is organized as follows: Section II briefly discusses CBFPs, the proposed algorithm is discussed in detail in Section III, followed by examples in Section IV. A brief discussion and contextualization of the obtained results, as well as some concluding remarks, are given in Section V.

II. Parameterized CBFPs

The aim of the parametric CBFP method [6] is to approximate the radiation pattern at an arbitrary point $\boldsymbol{x}^*$ in the

parameter space as

$$\boldsymbol{F}_r(\boldsymbol{x}^*) = \sum_{n=1}^{N} \alpha_n(\boldsymbol{x}^*)\boldsymbol{f}_n(\boldsymbol{x}_n), \tag{1}$$

where $\alpha_n(\boldsymbol{x}^*)$ is a function that yields the expansion coefficients at an arbitrary point $\boldsymbol{x}^*$ and $\boldsymbol{f}_n(\boldsymbol{x}_n)$ are the CBFPs, i.e., the pattern obtained through EM simulations at all points in the estimation set

$$\mathcal{X}^{\text{est}} = \{\boldsymbol{x}_1, \boldsymbol{x}_2, \cdots, \boldsymbol{x}_N\}. \tag{2}$$

Note that $\boldsymbol{x}_n$ is a vector consisting of an arbitrary combination of design variables, including frequency. The aim of this paper is to design an automated procedure that adaptively selects the points in $\mathcal{X}^{\text{est}}$ such that a parameterized pattern model, with controllable accuracy, is obtained.

Let $\mathbf{F}_{\text{M}}$ be an $N_p \times N$ matrix whose columns are the CBFPs in (1). A singular value decomposition (SVD) of $\mathbf{F}_{\text{M}}$ is then carried out, from which the first N_R ($N_R \leqslant N$) left-singular vectors of $\mathbf{F}_{\text{M}}$ are retained, constituting a (possibly) reduced set of CBFPs, denoted by $\mathbf{U}_{\text{R}} \in \mathbb{C}^{N_p \times N_R}$. The expansion coefficients corresponding to each CBFP (herein called the self-expansion coefficients) are the given by [6]

$$\boldsymbol{w}_n = [\mathbf{U}_{\text{R}}(\Omega_R)]^{\dagger}\boldsymbol{f}_n(\Omega_R), \tag{3}$$

where Ω_R is the set of N distinct directions, in the standard spherical coordinate system, in which the CBFPs are sampled. The superscript † indicates the pseudo-inverse of a matrix.

The self-expansion coefficients in (3) are column-stacked as

$$\mathbf{W} = [\boldsymbol{w}_1, \boldsymbol{w}_2, \cdots, \boldsymbol{w}_N], \tag{4}$$

and the expansion coefficients at an arbitrary point, $\boldsymbol{x}^*$, are then obtained as

$$\alpha_n(\boldsymbol{x}^*) = \mathcal{B}(\mathcal{X}^{\text{est}}, \boldsymbol{T}_n, \boldsymbol{x}^*), \tag{5}$$

where $\boldsymbol{T}_n$ represents the n-th row of $\mathbf{W}$ and $\mathcal{B}(\cdot)$ is an interpolating function [6]. Kriging [12] is used as the function, $\mathcal{B}(\cdot)$, throughout this paper, since it is well-suited to non-linear expansion over the global parameter space, with robust implementations available in, for instance, [13].

Once the expansion coefficients $\boldsymbol{\alpha} = [\alpha_1, \cdots, \alpha_N]$ are obtained from (5), the full radiation pattern may be recovered as detailed in [6].

III. Multivariate Adaptive Sampling

Like in many adaptive sampling algorithms, the goal is to select new sample points in potentially interesting regions of the parameter space. This could be regions with perceived rapid variation in the quantity of interest or simply large regions that are yet to be sampled. A multivariate adaptive sampling (MAS) algorithm is generally required to balance between *exploration* (i.e., adding points in large under-sampled regions) and *exploitation* (i.e., adding new points in regions of rapid function variation). These two properties are central to the development of several sequential sampling algorithms that have been used to tackle many important problems in different disciplines [14]–[17].

In what follows, we first describe the key steps involved in our formulation of the MAS algorithm, pertaining to the parameterized modeling of radiation patterns. We then proceed to adapt the proposed framework to include S-parameter dependence before discussing the convergence properties of the MAS algorithm.

A. Exploration

The goal of exploration is to add new points in under-sampled regions of the parameter space. This process is independent of the function (e.g., radiation patterns, scattering parameters, etc...) being modeled, and is only related to the coordinates of the current points in the parameter space.

Consider an N-dimensional parameter space, $\mathcal{P}$, with P sample points

$$\mathcal{X} = \{\boldsymbol{x}_1, \boldsymbol{x}_2, \cdots, \boldsymbol{x}_P\}. \tag{6}$$

The size of the region of $\mathcal{P}$ (i.e., the hypervolume) occupied by each point, $\{\boldsymbol{x}_k\}_{k=1}^{P}$, is computed in order to determine sparsely sampled regions. The hypervolume of each point is quantified by means of Voronoi tessellations [18]. A Voronoi tessellation of the parameter space, $\mathcal{P}$, containing the points in (6), consists of dividing $\mathcal{P}$ into $\{C_k\}_{k=1}^{P}$ cells, such that each cell C_k is a set of all points that are closer to the point $\boldsymbol{x}_k$ than any other point in $\mathcal{X}$.

The hypervolume, V_k, of the cell C_k is equivalent to the portion of the parameter space occupied by $\boldsymbol{x}_k$. A large V_k implies a sparsely sampled region while a small value indicates a densely sampled region of $\mathcal{P}$. An example of a Voronoi tessellation of a 2-D parameter space is shown in Fig. 1.

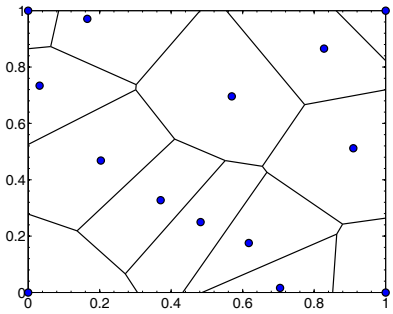

Fig. 1. Voronoi diagram of a 2-D parameter space. The line segments represent the boundaries of the Voronoi cells, C_k, for each point. The intersections of the line segments are the (well defined) Voronoi vertices that are used as candidate points as explained in Section III-B. The cells at the $x-$ and $y-$limits of the graph are not bounded.

The value of V_k can be computed exactly for bounded Voronoi diagrams. The cost of exact hypervolume computations does not scale well with the number of samples as well as dimension [19]. However, the cell volume, V_k, can be estimated accurately and cheaply using Monte Carlo simulations [15], [17], [19]. This approach is well suited for our purposes as it is fast (only involving fast point-wise operations like addition and subtraction) and scales well with the dimension of the parameter space. The cell volume estimation algorithm can be summarized as follows:

1) K points are uniformly randomly generated within the parameter space $\mathcal{P}$. We denote the set of the generated random points as $\mathcal{K}$.
2) Initialize $T_k \leftarrow 0$, where T_k is a counter for the number of points in $\mathcal{K}$ that are closest to $\boldsymbol{x}_k \in \mathcal{X}$, i.e., in the cell C_k.
3) For each point $\boldsymbol{p} \in \mathcal{K}$, compute the Euclidean distance with the points in $\mathcal{X}$ and set $T_k \leftarrow T_k+1$ if the randomly generated point, $\boldsymbol{p}$, is closest to $\boldsymbol{x}_k$.
4) The hypervolume, V_k, of each cell, C_k, is then estimated as $V_k \leftarrow \frac{T_k}{K}$.

The accuracy of the above algorithm depends on the number of random samples K. A value of $K = 100P$ was found to yield a sufficiently low error on the estimated hypervolume when compared to exact hypervolume computations [19], and this value is used throughout this paper. Cells with large volumes correspond to sparsely sampled regions and they are thus associated with high exploration scores.

B. Selection of Candidate Points

For a set of sample points in the parameter space, a Voronoi tessellation is performed and the *Voronoi vertices* (see Fig. 1) are selected as candidate points. We consider Voronoi vertices as the best candidate points for the MAS algorithm as they are a finite set of well-defined points that lie the farthest away from the current sample points, and are thus least influenced by the behavior of the function at the sample points.

C. Exploitation

Exploitation is the act of selecting new samples in regions of the parameter space where there are rapid function variations. To detect such regions, we use the principle of reflective exploration as described in [16], [20] and demonstrated in [11], for the 1-D case. An extension of the reflective exploration idea of [11] to the general N-dimensional (N-D) case is presented in this section.

Consider the set of points in (6), with $\boldsymbol{x}_P$ being the point from the latest simulation. Furthermore, consider a set of T candidate points

$$\mathcal{T} = \{\boldsymbol{p}_1, \cdots, \boldsymbol{p}_T\}, \tag{7}$$

obtained as described in Section III-B. Exploitation is then carried out according to the steps described below:

1) The radiation patterns corresponding to all points in $\mathcal{X}$ are column-stacked in a matrix $\mathbf{F}_\mathrm{M}$ and the self-expansion coefficients are computed and stored according to (3) and (4).
2) Let e_1 and e_2 denote the first and second rows of the matrix $\mathbf{W}$ in (4) (i.e., Vectors of the two dominant entries of the self-expansion coefficients). Let $\mathcal{M}^{(i)}_{\{h,l\}}$ denote a Kriging interpolant with e_i as the output, where $i \in \{1, 2\}$. The most accurate reflective function, $\mathcal{M}^{(i)}_h : \mathbb{R}^N \rightarrow \mathbb{R}$, is a Kriging interpolant trained on all points in $\mathcal{X}$. The other reflective function, $\mathcal{M}^{(i)}_l : \mathbb{R}^N \rightarrow \mathbb{R}$, is also a Kriging interpolant with training points $\mathcal{X} \setminus \{\boldsymbol{x}_P\}$ (i.e., all points except the most recent sample). In summary, two reflective functions are built for each of vectors e_1 and e_2.
3) Let $\mathcal{V} \subset \mathcal{T}$ be the set of Voronoi vertices belonging to C_P, the Voronoi cell that has the latest point, $\boldsymbol{x}_P$, as an interior point. The points in $\mathcal{V}$ are closest to $\boldsymbol{x}_P$ and hence are considered to be biased towards $\mathcal{M}_h$, since $\mathcal{M}_l$ has no information in this region. A new set of candidate points is thus obtained as $\mathcal{T}_{new} = \mathcal{T} \setminus \mathcal{V}$. This step is a generalization from the 1-D case, where points in a segment were ignored (see [11]), to the N-D case, where points in a hypervolume are ignored.
4) The functions $\mathcal{M}^{(i)}_h$ and $\mathcal{M}^{(i)}_l$ are evaluated on the candidate points in $\mathcal{T}_{new}$ and the difference between the two reflective functions is computed. A region of rapid function variation contains the point in $\mathcal{T}_{new}$ at which $\left|\mathcal{M}^{(i)}_h - \mathcal{M}^{(i)}_l\right|$ is maximum, as an interior point.

Reflective functions, of the same form as the one in (5), are used to estimate the locations of regions of fast variations, in contrast to the local linear approximation technique used in [14], [15], [17]. The clear advantage of the proposed approach is that the dynamics of the model are taken into account as regions of non-linear variation, that may not be detected by the linear approximation method, are readily handled by the non-linear reflective functions.

D. Inclusion of S-parameters

We first remark that S-parameter dependence is, in general, polynomial in geometric parameters and rational in frequency. In light of the above observation, the multivariate modeling of S-parameters can be accomplished by means of standard techniques from the parametric macromodeling literature [21]–[23]. These techniques however require the treatment of frequency as a special parameter, i.e., running EM simulations at multiple frequency points for each fixed geometry. Other multivariate adaptive sampling techniques for S-parameters, based on rational functions, include [24], [25].

In order to easily integrate S-parameter modeling in the same paradigm as that of radiation patterns, with similar candidate point selection as well as exploration/exploitation features, Kriging is chosen as the fitting function as in [15].

The exploitation technique, in Section III-C, is used (with the obvious modification that the magnitude of the actual S-parameter magnitude values are used as function outputs) in order to quantify S-parameter variation over the parameter space.

E. Ranking and Sample Selection

1) Exploitation Score: The exploitation score is computed, for radiation patterns, for each of the candidate points in $\mathcal{T}_{new}$. First, we identify whether the normalized maximum difference $\left|\mathcal{M}^{(i)}_h - \mathcal{M}^{(i)}_l\right| / \max\{|\mathcal{M}^{(i)}_h|\}$, occurs for $i = 1$ or $i = 2$, and we denote this value of i as j. Next, we only consider the models $\mathcal{M}^{(j)}_{\{h,l\}}$ and compute a normalized exploitation score for each of the candidate points as

$$Q^r(\boldsymbol{p}_t) = \frac{\overline{Q^r}(\boldsymbol{p}_t)}{\sum_{t=1}^{T_{new}} \overline{Q^r}(\boldsymbol{p}_t)}, \tag{8}$$

where $\overline{Q^r}(\boldsymbol{p}_t) = \left|\mathcal{M}_h^{(j)} - \mathcal{M}_l^{(j)}\right|$, with $\mathcal{M}_{\{h,l\}}^{(j)}$ being Kriging functions (of CBFP coefficients) evaluated at $\boldsymbol{p}_t$ and $t = \{1, 2, \cdots, T_{new}\}$, with T_{new} being the number of points in $\mathcal{T}_{new}$.

Similarly, the exploitation score for S-parameters is computed as

$$Q^s(\boldsymbol{p}_t) = \frac{\overline{Q^s}(\boldsymbol{p}_t)}{\sum_{t=1}^{T_{new}} \overline{Q^s}(\boldsymbol{p}_t)}, \tag{9}$$

where $\overline{Q^s}(\boldsymbol{p}_t) = |\mathcal{M}_h - \mathcal{M}_l|$, with $\mathcal{M}_{\{h,l\}}$ being the Kriging functions (of S-parameters) evaluated $\forall \boldsymbol{p}_t \in \mathcal{T}_{new}$.

2) Exploration Score: The exploration score consists of first computing the hypervolume of each candidate point when added to the set of current points in the parameter space (6). A normalized exploration score is then obtained as

$$V(\boldsymbol{p}_t) = \frac{\overline{V}(\boldsymbol{p}_t)}{\sum_{t=1}^{T_{new}} \overline{V}(\boldsymbol{p}_t)}, \tag{10}$$

where $\overline{V}(\boldsymbol{p}_t)$ is the hypervolume of the Voronoi cell containing the point $\boldsymbol{p}_t \in \mathcal{T}_{new}$. Note that, ideally, (10) is computed for each candidate point on the set $\mathcal{X} \cup \{\boldsymbol{p}_t\}$. However, from a practical implementation vantage point, the sequential computation of the cell volume (e.g., in a `for` loop), for each point $\{\boldsymbol{p}_t\}$, is an unacceptably slow process as the number of sample points in $\mathcal{X}$ (and hence the number of candidate points) or the problem's dimension increases, sometimes being slower than an EM simulation. Therefore, the cell volumes are computed at once using the set $\mathcal{X} \cup \mathcal{T}_{new}$. This is motivated by the fact that the tessellation around two different points are independent of each other if the points are distant. Since very close candidate points are likely to have similar exploitation scores, the errors introduced by cell volume computations are mitigated from a ranking perspective. As such, the time benefits clearly outweigh accuracy concerns and thus justifying this design decision.

3) Ranking and Selection: Having computed the exploration and exploitation scores, the ranking of candidate points is quantified as

$$R(\boldsymbol{p}_t) = \beta_1 Q^r(\boldsymbol{p}_t) + \beta_2 Q^s(\boldsymbol{p}_t) + \beta_3 V(\boldsymbol{p}_t), \tag{11}$$

where $t = \{1, 2, \cdots, T_{new}\}$, $\beta_i \in [0, 1]$ for $i \in \{1, 2, 3\}$ and the sample point to be simulated next is the candidate point $\boldsymbol{p}_t$ at which (11) is maximum. The simple formulation of the ranking score in (11) allows a great deal of flexibility as the same algorithm can be easily biased towards either exploration or exploitation by varying the values of the weights β_i.

F. On the Stopping Criterion of the MAS Algorithm

The goal of the MAS method is to generate parameterized models of radiation patterns and S-parameters.

Concerning radiation patterns, the algorithm first seeks a set of CBFPs that span the subspace of all radiation patterns in an asymptotic sense (i.e., there's little variation in the energy of the smallest singular value as more basis functions are added). Then it only remains to guarantee the accuracy of linear combinations of CBFPs for an accurate pattern model to be obtained. The first criterion is typically achieved when $\frac{\sigma_{\min}}{\sigma_{\max}} < 10^{-10}$, where $\sigma_{\min}$ and $\sigma_{\max}$ are the minimum and maximum singular values of $\mathbf{F}_{\mathrm{M}}$ as shown in Fig. 2. The second criterion is achieved when

$$\mathcal{H}\left\{\max\left\{\left|\frac{\mathcal{M}_h^{(j)} - \mathcal{M}_l^{(j)}}{\mathcal{M}_h^{(j)}}\right|\right\}\right\} < \lambda_1, \tag{12}$$

where $\mathcal{H}\{\cdot\}$ is a moving average function, with a window size of about 30, and λ_1 is a preset tolerance.

Concerning S-parameters, an accurate model is obtained when

$$\mathcal{H}\left\{\max\left\{\left|\frac{\mathcal{M}_h^{s} - \mathcal{M}_l^{s}}{\mathcal{M}_h^{s}}\right|\right\}\right\} < \lambda_2, \tag{13}$$

where λ_2 is a pre-set tolerance.

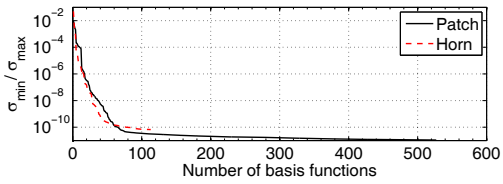

Fig. 2. SVD spectra for the two antennas discussed in Section IV. The slow variation below 10^{-10} can be clearly seen.

The averaging functions in (12) and (13) are smooth monotonically decreasing approximations of the true error (i.e., difference between reflective functions). The true error function is not smooth due to changing candidate points from one iteration to another as shown in Fig. 5. Since $\mathcal{H}\{\cdot\}$ is smooth and decreasing, the stopping criteria $\lambda_{\{1,2\}}$ can be chosen to be small in order to ensure that all relevant features of the reflective functions are captured over the design space (in line with standard reflective exploration principles). Our experiments on various antennas suggest that values of $\lambda_{\{1,2\}} < 10^{-1}$ are sufficient in order to obtain accurate models.

The MAS algorithm converges when the expressions in (12) and (13) are both satisfied n times (where n is a small integer), to build some robustness into the algorithm. The values of $\lambda_{\{1,2\}}$ can effectively be used to control the approximation error of the models built with the generated basis functions. Note that, in order to avoid false positives (in terms of convergence), conditions (12) and (13) are only checked after $\frac{\sigma_{\min}}{\sigma_{\max}} < 10^{-10}$ is satisfied.

Given the starting set of points in (6), the MAS algorithm can be summarized as follows: (i) select candidate points; (ii) compute the exploration score; (iii) compute the exploitation score; (iv) compute the ranking score and select the candidate point with maximum ranking score as the next sample to evaluate; and finally (v) repeat steps (i)–(iv) until the stopping criterion is reached.

Pertinent numerical examples are provided in the next section to validate the proposed MAS algorithm.

IV. Numerical Examples

The MAS algorithm is implemented in MATLAB [26] and the open-source DACE toolbox [13] is used for Kriging. Two relevant examples are presented in this section. The first

involves a horn antenna operating near the cut-off frequency of its input waveguide. The other example involves an aperture-coupled patch antenna with six variables. All antennas are simulated using FEKO, a commercial method of moments code [27].

The relative root mean square error (RRMSE) between the model and validation data samples is used to assess modeling accuracy of the radiation patterns. The RRMSE is given by

$$E(s) = \sqrt{\frac{\sum_{k=1}^{N_d} \left| G_k - \widetilde{G}_k \right|^2}{\sum_{k=1}^{N_d} |G_k|^2}}, \qquad (14)$$

where G_k is the validation data and $\widetilde{G}_k$ is the prediction from the model. Note that G_k and $\widetilde{G}_k$ are generic variables that denote either magnitude or the phase of the co-polarized electric field. S-parameter modeling accuracy is assessed through absolute difference errors between model and validation samples.

A. Horn Near Cut-Off

A horn with three corrugations, shown in Fig. 3, is investigated in this example. The diameter of the horn's input waveguide is $d_c = 0.19$ m (which has a cut-off frequency of 0.92 GHz for the fundamental TE_{11} mode). The investigated example is a bivariate problem, with the variables being the flare angle of the horn $a_c \in [0°, 7°]$ and frequency $f \in [0.95, 1.20]$ GHz. The antenna's directivity, at broadside, varies in a highly non-linear manner, between 2.5 dB and 11 dB. The shape of the radiation pattern also varies significantly over this parameter space.

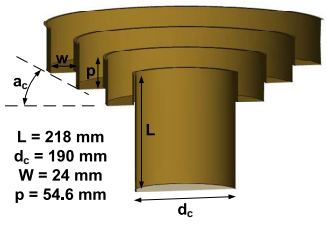

Fig. 3. Simulation model of an axially corrugated choke horn.

The MAS algorithm is executed starting from 10 points, with $\beta_i = 1\ \forall i$ in (11), until the stopping criteria of $\lambda_1 = \lambda_2 = 10^{-3}$ is reached, which required an additional 103 samples selected adaptively. The pattern and S-parameter models are constructed using Kriging as the interpolation kernel where a Matérn $\frac{5}{2}$ correlation function [28] is used. The resulting models are validated over a dense grid of 1024 points and the pattern results are depicted in Fig. 4 for selected points in the validation set.

The convergence rate of the MAS algorithm is shown in Fig. 5, where it is apparent that the true error, (12) with no averaging, is unsuitable to be used for convergence purposes (i.e., it has many peaks). The averaged pattern error function is shown to be smooth and monotonically decreasing until the criterion of $\lambda_{\{1,2\}} < 10^{-3}$ is satisfied. The S-parameter error function follows a similar trend.

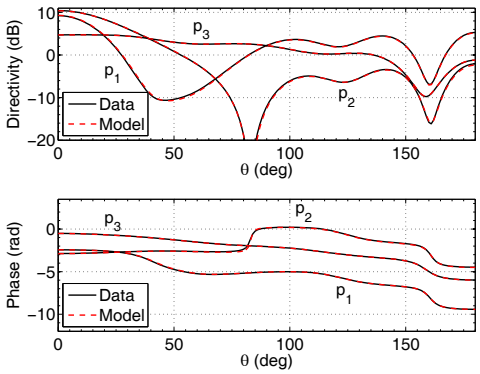

Fig. 4. Horn: Directivity (top panel) and phase (bottom panel) plots of the pattern in the $\phi = 90°$ plane, for $p_1 = \{2.754, 1.125\}; p_2 = \{1.843, 1.156\}$ and $p_3 = \{3.459, 0.963\}$. The non-linear variation of the pattern is obvious.

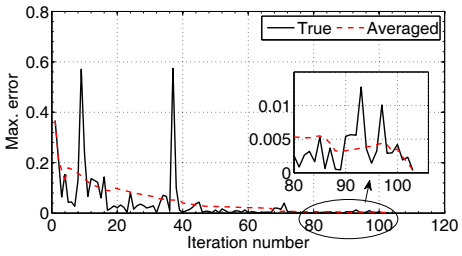

Fig. 5. Horn: Convergence of pattern error function (12) of MAS algorithm. The true error is not smooth due to changing sets of candidate points between iterations. A smooth and decreasing averaged error can be clearly seen. The S-parameter error function (13) behaves similarly.

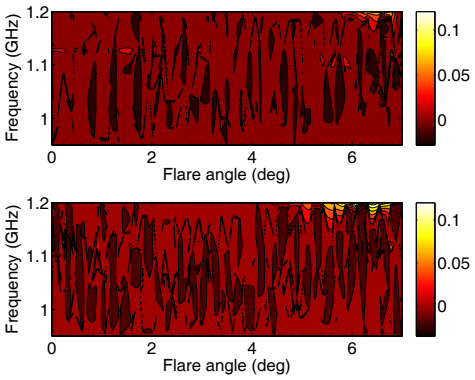

Fig. 6. Horn: Maximum directivity error for 113 points selected with MAS (top panel) and 150 points selected with LHS (bottom panel). It is evident that a better model is obtained with the proposed MAS technique.

To illustrate the effectiveness of our approach, a comparison is made between the model obtained with the MAS technique with a model obtained using 150 points generated by means of LHS. The maximum magnitude modeling errors are 0.089 and 0.126 for the MAS and LHS models respectively (the corresponding maximum phase errors are 0.96 and 0.90). The magnitude modeling errors are shown in Fig. 6 which demonstrates that a better model is obtained with fewer points with our proposed approach than with common LHS based sampling schemes. Moreover, owing to the stochastic nature of LHS, no measure of error control can be guaranteed, i.e., an LHS-based distribution of a specified number of points may or

may not yield a sufficiently accurate model (unless the data set is large). In contrast, the proposed MAS algorithm guarantees models of arbitrary accuracy as desired by a user.

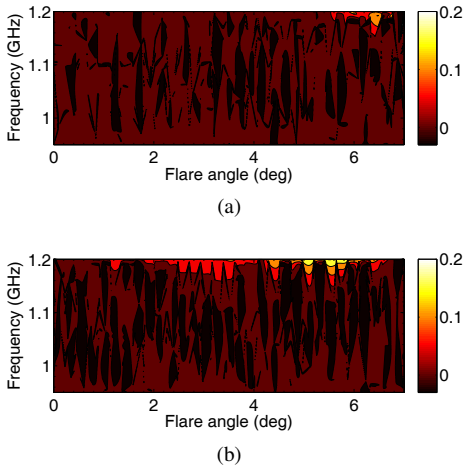

Fig. 7. Absolute difference error between model and validation data: (a) MAS, (b) LHS. The maximum, mean and median errors are 0.16, 45×10^{-3} and 18×10^{-3} for MAS; and 0.18, 76×10^{-3} and 18×10^{-3} for LHS respectively.

The accuracy of the S-parameter model is shown in Fig. 7, where low absolute errors can be observed over the parameter space. The maximum absolute difference error obtained with an LHS-based model (with 150 samples) is 0.184 compared to 0.163 with MAS, further highlighting the superior performance of the proposed MAS algorithm, even with fewer samples.

Fig. 8 shows contour plots of the variation of S-parameters and e_2 (see Section III-C) as well as the samples selected by the MAS algorithm for different values of the weighting factors β_i in (11). A higher concentration of samples can be clearly seen in regions of more dynamic variations of the pattern (represented by the self-expansion coefficients e_2) or S-parameters. All models in Fig. 8 are validated over the same set of 1024 points and details about convergence and validation errors are reported in Table I, including pattern and S-parameter models built using exploitation only.

TABLE I
MODELING DETAILS FOR DIFFERENT WEIGHTING FACTORS. THE REPORTED ERRORS ARE RRMSE AND ABSOLUTE DIFFERENCE FOR THE PATTERN AND S-PARAMETERS RESPECTIVELY.

Weights			Criteria		Max. Error		#
β_1	β_2	β_3	λ_1	λ_2	Pattern	S-param.	Points
1	0	1	10^{-3}	N/A	0.114	0.176	100
0	1	1	N/A	10^{-3}	0.202	0.053	105
1	1	1	10^{-3}	10^{-3}	0.089	0.168	113
1	1	0	10^{-3}	10^{-3}	0.092	0.162	118

The expected error variation is observed for the first two cases in Table I, while a comparison of the last two cases shows that, with the exploitation-only approach, some potentially dynamic regions of the parameter space may be left unexplored. This resulted in a 4.4% increase in the number of selected samples relative to the case where sample selection is carried out using both exploitation and exploration scores.

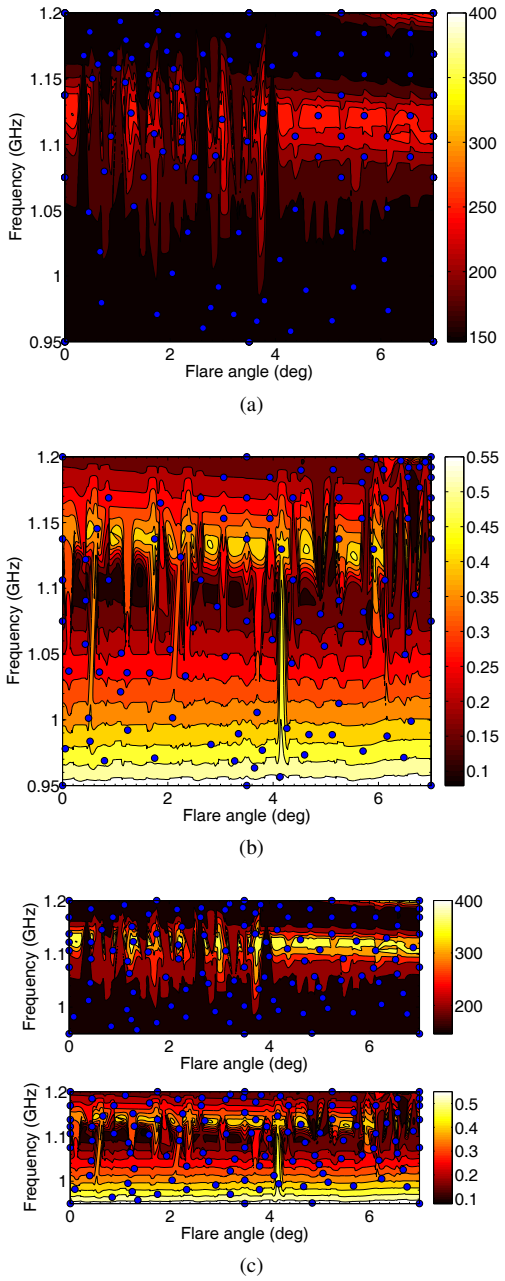

Fig. 8. Horn: Sample distributions (shown as •) for different weighting factors. (a) Variation of e_2 and selected samples with weighting factors $\beta_1 = 1, \beta_2 = 0, \beta_3 = 1$ – pattern modeling only. (b) Variation of the magnitude of S-parameters and selected samples with weighting factors $\beta_1 = 0, \beta_2 = 1, \beta_3 = 1$ – S-parameter modeling only. (c) Variation of e_2 (top panel) and S-parameter variation (bottom panel) for balanced weighting factors $\beta_1 = 1, \beta_2 = 1, \beta_3 = 1$ – combined pattern and S-parameter modeling. Higher sample densities in regions of fast function variation can clearly be seen in all figures. We stress that only one (e_2) of the two coefficients (e_1, e_2) necessary to quantify pattern variations is shown in (a) and (c).

B. Aperture Coupled Patch

An aperture coupled patch antenna, shown in Fig. 9, is investigated in this example. The model consists of 6 variables that are described in Fig. 9.

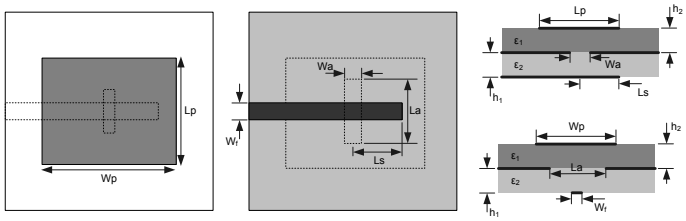

Fig. 9. Detailed geometry of the aperture coupled antenna. The variables involved are: $W_\mathrm{a} \in [1.2, 1.8]$ mm; $L_\mathrm{a} \in [35, 46.5]$ mm; $L_\mathrm{s} \in [6, 8]$ mm; $L_\mathrm{p} \in [50, 60]$ mm; $W_\mathrm{p} \in [65, 80]$ mm and $f \in [1.6, 2.4]$ GHz. The remaining parameters are fixed at $h_1 = 1.5$ mm, $h_1 = 12$ mm, $\varepsilon_1 = 1$, $\varepsilon_2 = 4.3$ and $W_\mathrm{f} = 3$ mm.

The adaptive sampling algorithm is executed by starting with 75 points (including corner points) selected with LHS, and the convergence parameters are set as $\lambda_1 = \lambda_2 = 5{\times}10^{-2}$. The algorithm is set to converge after the parameters λ_1 and λ_2 are reached a number of $n = 2$ times, and this requires a total of 625 samples.

The model is built as in Section IV-A and it is validated on a set of 300 points and the error distribution is shown in Fig. 10, where it can clearly be seen that models with large errors are outliers. A comparison between the pattern model and validation data, selected as points with median error in the validation set, is shown in Fig. 11, where a good agreement can be observed.

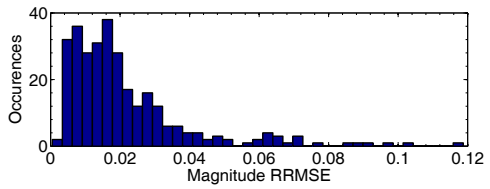

Fig. 10. Patch: Magnitude error distribution over a validation set of 300 samples.

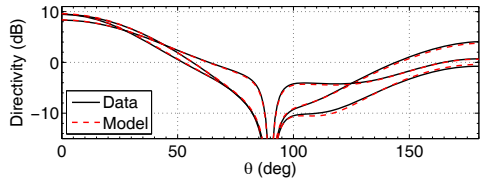

Fig. 11. Patch: Accuracy of the radiation pattern model at selected points in the validation set, in the $\phi = 45°$ plane.

The maximum absolute difference error in the model of the associated S-parameters is 0.095 over the validation set, with mean and median absolute errors given by 0.018 and 0.012 respectively. Fig. 12 shows a comparison between model and data at selected points with median errors in the validation set and a relatively good agreement can be observed between various curves.

V. Discussion

We remind the reader that traditional frequency domain EM simulations are repeatedly carried out at multiple frequency points for a fixed geometry. Such wide band simulations may be enhanced by using adaptive frequency sampling (AFS) algorithms such as [11], [29], leading to a reduced computational cost. The proposed method treats frequency like an ordinary parameter and optimally places samples in the subspace of geometric parameters and frequency. As such, the computational cost of the proposed method in Section IV-A is equivalent to about 11 traditional EM simulations (i.e., a fixed geometry is simulated at a number of frequency points), enhanced with the AFS method in [11] (the mean number of frequency points selected using [11], on 10 different geometries of the antenna, is about 10). For the example in Section IV-B, the equivalent computational cost is only about 40 traditional simulations (also enhanced with adaptive frequency sampling), a very small number for a 5-D problem. Note that far fewer samples are required in cases where frequency variation is not included or for narrow band models.

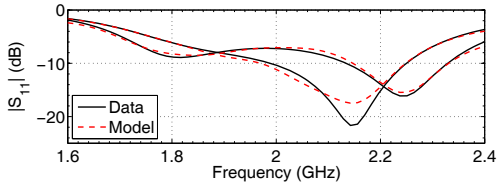

Fig. 12. Patch: S-parameter data vs model at selected validation points.

Therefore the proposed method allows one to obtain more information about the variation of the antenna's output characteristics, as a function of design parameters, at a fraction of the computational cost, compared to when the same antenna is modeled using traditional techniques. Additionally, the proposed method adaptively constructs a single model for the full radiation pattern, thereby avoiding the need for building separate models for each figure of merit (e.g., directivity, cross-polarization, side lobe levels). Indeed, the outcome of the proposed technique is a single model that fully characterizes an antenna. Furthermore, the models are constructed without *a priori* knowledge of the pattern or S-parameter variation over the design space. The obtained model is quick to evaluate ($\sim$ 0.2 s) and may be efficiently used for computationally expensive design activities like optimization and sensitivity analysis. Moreover, the models in Section IV have a controllable approximation error that is determined by the values of λ_1 and λ_2. Note that λ_1 and λ_2 in (12) and (13) are normalized values and thus are independent of the particular antenna under consideration. We however suggest values of $\lambda_{\{1,2\}} \leqslant 5 \times 10^{-2}$ in order to obtained sufficiently accurate models, with lower values leading to better accuracy and at the cost of increased numbers of EM simulations.

Although the discussion on S-parameters is limited to the input reflection coefficient, the basic framework can be extended to multiport systems by modeling the variation of each entry of the scattering matrix with a pair of reflective functions, similarly to what was done for the self-expansion coefficients of the radiation pattern in Section III-C.

In terms of algorithm complexity and scalability, the underlying Kriging interpolation complexity scales as $O(N^3)$, and

is typically only suitable for parameter spaces up to about 10-dimensions. However, the main bottleneck normally remains the absolute number of samples, since the simulation times are typically much slower than model building.

Finally, work is ongoing to determine the sensitivity of the algorithm to noise in the data. Since the SVD often results in an over-determined system, we expect the algorithm to be relatively robust to noisy data.

REFERENCES

[1] S. Ulaganathan, S. Koziel, A. Bekasiewicz, I. Couckuyt, E. Laermans and T. Dhaene, "Cost-efficient modeling of antenna structures using gradient-enhanced Kriging," in *2015 Loughborough Antennas Propag. Conf. (LAPC),* Nov. 2015, pp. 1–5.

[2] J. P. Jacobs, "Bayesian support vector regression with automatic relevance determination kernel for modeling of antenna input characteristics," *IEEE Trans. Antennas Propag.*, vol. 60, no. 4, pp. 2114–2118, Apr. 2012.

[3] S. Koziel, S. Ogurtsov, I. Couckuyt and T. Dhaene, "Variable-fidelity electromagnetic simulations and co-Kriging for accurate modeling of antennas," *IEEE Trans. Antennas Propag.*, vol. 61, no. 3, pp. 1301–1308, Mar. 2013.

[4] S. Koziel and S. Ogurtsov, "Multi-objective design of antennas using variable-fidelity simulations and surrogate models," *IEEE Trans. Antennas Propag.*, vol. 61, no. 12, pp. 5931–5939, Dec. 2013.

[5] D. I. L. de Villiers, "Fast parametric modeling of radio astronomy reflector antenna noise temperature," *IEEE Trans. Antennas Propag.*, vol. 64, no. 6,pp. 2522–2526, June 2016.

[6] N. Mutonkole, E. R. Samuel, D. I. L. de Villiers and T. Dhaene, "Parametric modeling of radiation patterns and scattering parameters of antennas," *IEEE Trans. Antennas Propag.*, vol. 64, no. 3, pp. 1023–1031, Mar. 2016.

[7] A. Young, R. Maaskant, M. V. Ivashina, D. I. L. de Villiers and D. B. Davidson, "Accurate beam prediction through characteristic basis function patterns for the MeerKAT/SKA radio telescope antenna," *IEEE Trans. Antennas Propag.*, vol. 61, no. 5, pp. 2466–2473, May 2013.

[8] N. Mutonkole and D. I. L. de Villiers, "Characteristic basis function patterns method for reflector antenna calibration: an extension to multiple frequencies," in *9th Eur. Conf. Antennas Propag. (EuCAP)*, Lisbon, Portugal, Apr. 2015, pp. 1–5.

[9] G. Giordanengo, M. Righero, F. Vipiana, G. Vecchi and M. Sabbadini, "Fast antenna testing with reduced near field sampling," *IEEE Trans. Antennas Propag.*, vol. 62, no. 5, pp. 2501–2513, May 2014.

[10] M. D. McKay, R. J. Beckman and W. J. Conover, "A comparison of three methods for selecting values of input variables in the analysis of output from a computer code," *Technometrics*, vol. 42, no. 1, pp. 55–61, Feb. 2000.

[11] N. Mutonkole and D. I. L. de Villiers, "An adaptive sampling algorithm for the efficient prediction of antenna radiation patterns over a wide frequency bandwidth," in *10th Eur. Conf. Antennas Propag. (EuCAP)*, Davos, Switzerland, Apr. 2015, pp. 1–5.

[12] J. P. C. Kleijnen, *Design and analysis of simulation experiments*, New York: Springer, 2008.

[13] DACE: A MATLAB Kriging Toolbox. [Online]. Available: http://www2.imm.dtu.dk/ hbni/dace/

[14] D. Deschrijver, F. Vanhee, D. Pissoort and T. Dhaene, "Automated near-field scanning algorithm for the EMC analysis of electronic devices," *IEEE Trans. Electromgan. Compat.*, vol. 54, no. 3, pp. 502–510, June 2012.

[15] D. Deschrijver, K. Crombecq, H.M. Nguyen and T. Dhaene, "Adaptive sampling algorithm for macromodeling of parameterized S-parameter responses," *IEEE Trans. Microw. Theory Tech.*, vol. 59, no. 1, pp. 39–45, Jan. 2011.

[16] J. De Geest, T. Dhaene, N. Fache and D. De Zutter, "Adaptive CAD-model building algorithm for general planar microwave structures," *IEEE Trans. Microw. Theory Tech.*, vol. 47, no. 9, pp. 1801–1809, Sep. 1999.

[17] K. Crombecq, D. Gorissen, D. Deschrijver and T. Dhaene, "A novel hybrid sequential design strategy for global surrogate modeling of computer experiments," *SIAM J. Sci. Comput.*, vol. 33, no. 4, pp. 1948–1974, 2011.

[18] F. Aurenhammer, "Voronoi diagrams – a survey of a fundamental geometric data structure," *ACM Comput. Surveys*, vol. 23, no. 3, pp. 345–405, 1991.

[19] K. Crombecq, "Surrogate modelling of computer experiments with sequential experimental design," Ph.D. dissertation, university of Antwerp, Antwerp, Belgium, 2012.

[20] E.R. Samuel, F. Ferranti, L. Knockaert and T. Dhaene, "A hybrid adaptive sampling algorithm for obtaining reduced order models for systems with frequency dependent state-space matrices," *Int. J. Numer. Model.*, vol. 29, no. 4, pp. 741–754, July 2016.

[21] D. Deschrijver, T. Dhaene, and D. De Zutter, "Robust parametric macro-modeling using multivariate orthonormal vector fitting," *IEEE Trans. Microw. Theory Tech.*, vol. 56, no. 7, pp. 1661–1667, July 2008.

[22] P. Triverio, S. Grivet-Talocia and M. S. Nakhla, "A parameterized macromodeling strategy with uniform stability test," *IEEE Trans. Adv. Packag.*, vol. 32, no. 1, pp. 205–215, Feb. 2009.

[23] E.R. Samuel, L. Knockaert, F. Ferranti, and T. Dhaene, "Guaranteed Passive Parameterized Macromodeling by Using Sylvester State-Space Realizations," *IEEE Trans. Microw. Theory Tech.*, vol. 61, no. 4, pp. 1444-1454, Apr. 2013.

[24] A. Cuyt, R. B. Lenin, S. Becuwe and B. Verdonk, "Adaptive multivariate rational data fitting with applications in electromagnetics," *IEEE Trans. Microw. Theory Tech.*, vol. 54, no. 5, pp. 2265–2274, May 2006.

[25] R. Lehmensiek and P. Meyer, "Creating accurate multivariate rational interpolation models of microwave circuits by using efficient adaptive sampling to minimize the number of computational electromagnetic analyses," *IEEE Trans. Microw. Theory Tech.*, vol. 49, no. 8, pp. 1419–1430, Aug. 2001.

[26] MATLAB R2009A User's Guide. [Online]. Available: www.mathworks.com

[27] FEKO version 7.0. Altair HyperWorks. Stellenbosch, South Africa, 2015. [Online]. www.feko.info

[28] S. Ulaganathan, I. Couckuyt, F. Ferranti, T. Dhaene and E. Laermans, "Variable-fidelity surrogate modelling with Kriging," in *Proc. 17th Int. Conf. Chemistry and Chemical Eng.*, Amsterdam, The Netherlands, 2015, pp. 514–518.

[29] T. Dhaene, J. Ureel, N. Fache and D. De Zutter, "Adaptive frequency sampling algorithm for fast and accurate S-parameter modeling of general planar structures," in *IEEE MTT-S Int. Microw. Symp. Dig.*, vol. 3, May 1995,pp. 1427–1430.

Ngoy Mutonkole received the B.Eng., M.Eng. and Ph.D. degrees in electrical and electronic engineering from the University of Stellenbosch, Stellenbosch, South Africa, in 2011, 2013 and 2016 respectively. He is currently with Altair Engineering GmbH, Boeblingen, Germany, where he works as an engineer involved in Software Integrity as well as in the development of optimization algorithms for microwave devices.

His current research interests include machine learning, surrogate based modeling and optimization techniques with applications to the design of antennas and other RF/microwave devices.

Dirk I. L. de Villiers (S'05-M'08-SM'15) received the B.Eng and Ph.D. degrees in electrical and electronic engineering from the University of Stellenbosch, Stellenbosch, South Africa in 2004 and 2007 respectively.

From 2008 to 2009 he was a post-doctoral fellow at the University of Stellenbosch working on antenna feeds for the South African SKA program. He is currently an Associate Professor at the University of Stellenbosch, and has spent several months as visiting researcher at Antwerp University in Antwerp, Belgium, at Chalmers University of Technology in Gothenburg, Sweden, as well as at the University of Novi Sad in Serbia. Between 2010 and 2014 he has worked on contract for EMSS Antennas (Pty) Ltd in Stellenbosch, South Africa, on the design of the reflector optics for the MeerKAT and SKA radio telescopes. His main research interests include reflector antennas as well as the design of microwave components.

He currently serves as chair of the South African IEEE joint AP/MTT/EMC chapter.